Specific heat of liquid ^{3}He under pressure in a restricted geometry

R. Schrenk* and R. König
Physikalisches Institut, Universität Bayreuth, D-95440 Bayreuth, Germany
(Received 12 May 1997; revised manuscript received 27 October 1997)

We have investigated the specific heat of liquid ^{3}He confined to an Ag sinter with an average pore size of about 1000 Å in the temperature range 1 mK$\leqslant T \leqslant$20 mK and at pressures 4.8 bar$\leqslant p \leqslant$34.0 bar. The specific heat of normal-fluid ^{3}He in the sinter pores shows the linear temperature dependence expected for a Fermi liquid. However, the effective mass of the ^{3}He quasiparticles is clearly enhanced in the restricted geometry compared to data obtained in bulk ^{3}He. In addition, there is a temperature-independent contribution to the specific heat, the origin of which can be interpreted as the specific heat of the second layer of ^{3}He on the Ag surface. Moreover, compared with the results obtained for bulk ^{3}He, we observe a much broader maximum in the specific heat in the vicinity of the superfluid transition; this maximum occurs about 0.4 mK below the bulk superfluid transition temperature. Furthermore, in the confinement of the sinter only a part of the ^{3}He in the sinter (about 60%) becomes superfluid. In contrast to the results obtained with pure ^{3}He the specific heat of a liquid ^{3}He-^{4}He mixture (1% ^{3}He) in the Ag sinter shows no deviation from bulk data. [S0163-1829(98)03314-1]

I. INTRODUCTION

At temperatures below about one-tenth of the Fermi temperature T_F (which is about 1 K in ^{3}He), the static and dynamic properties of liquid ^{3}He in its normal-fluid phase are well described by the phenomenological Landau Fermi-liquid theory.[1] In this temperature range, ^{3}He may be treated as a degenerate Fermi liquid, and the interaction among the ^{3}He quasiparticles is described by the so-called Fermi-liquid parameters, which have to be derived from experiment. The temperature dependences predicted by Landau's Fermi-liquid theory for the specific heat ($C \sim T$), thermal conductivity ($\kappa \sim T^{-1}$), spin diffusion ($D \sim T^{-2}$), and viscosity ($\eta \sim T^{-2}$) of liquid ^{3}He in the degenerate regime result from the fermionic nature of the ^{3}He quasiparticles and the Pauli exclusion principle for scattering of spin-$\frac{1}{2}$ particles around the Fermi sphere.[2] In particular, the dynamic properties of liquid ^{3}He with their distinct temperature dependences are very sensitive tools for studying the interaction among ^{3}He quasiparticles and for providing information about the Fermi-liquid parameters in the degenerate regime.

The Landau Fermi-liquid theory predicts a specific heat of normal-fluid ^{3}He that is linearly dependent on temperature in the degenerate regime. The coefficient of the specific heat is proportional to the effective mass m_3^* of the ^{3}He quasiparticles, which is a measure of the interaction between the ^{3}He quasiparticles and is therefore strongly dependent on the pressure the sample is exposed to. The quasiparticle interaction, in turn, may be influenced by different length scales, depending on whether ^{3}He is in its normal-fluid or in its superfluid state.

The dominating length scale for the quasiparticle interaction in normal-fluid ^{3}He is given by the mean free path λ of the ^{3}He quasiparticles. According to Landau's theory of Fermi liquids, λ follows a T^{-2} law in the degenerate regime; its magnitude is of the order of $\sim$0.1 μm at about 30 mK and increases to almost 100 μm at $T=1$ mK. In the superfluid state, the characteristic length scale of ^{3}He is the pressure-dependent coherence length $\xi(p)$, which is a measure for the spacial expansion of the Cooper pairs. At T_C, the superfluid transition temperature, the coherence length becomes infinite and decreases with decreasing temperature to values of a few 100 Å.

The properties of a system are influenced by a restricted geometry, when the dimension of the confinement becomes comparable to the characteristic lengths of the system. In particular, in liquid ^{3}He the superfluid phase transition is suppressed, and the superfluid fraction decreases in a confining geometry.[3] In normal-fluid ^{3}He, an increase of the effective mass of the ^{3}He quasiparticles was observed in various restricted geometries.[4] We report on experiments in which pure ^{3}He is confined to the pores of an Ag sinter with an average pore size of $\sim$1000 Å. As already mentioned above, this dimension of the restricted geometry becomes comparable to the characteristic lengths of normal-fluid and superfluid ^{3}He in the temperature range of our experiment and we therefore may expect to observe an impact of this confinement on the properties of our ^{3}He sample.

A different system for the investigation of the interaction among ^{3}He quasiparticles is provided by liquid ^{3}He-^{4}He mixtures due to the finite solubility of ^{3}He in superfluid ^{4}He at ^{3}He concentrations x_3 less than 6.4% at zero pressure[5] and up to 9.5% at $p=10$ bar[6] even at $T=0$ K. In liquid ^{3}He-^{4}He mixtures, the Fermi temperature and therefore the Fermi-liquid regime is not only influenced by the pressure of the mixture but mainly by the concentration of the ^{3}He component. In the degenerate regime of the mixtures, the properties of the system are determined by the properties of the ^{3}He component; the superfluid ^{4}He acts only as an inert background on the effective mass of the ^{3}He quasiparticles. In addition to our measurements on pure ^{3}He, we have measured the specific heat of a liquid ^{3}He-^{4}He mixture with a ^{3}He concentration $x_3=1.0\%$ at two different pressures ($p=0$ and 21.0 bar) and confined to the same Ag sinter as a

 © 1998 The American Physical Society

reference system with a much weaker quasiparticle interaction than in pure ^{3}He.

In the next section, the experimental setup is described. In Sec. III, we present and discuss the results for the specific heat of pure liquid ^{3}He confined to the sinter pores; these data were taken at $p=4.8$, 15.5, 25.2, and 34.0 bar. We compare our findings with our results for the specific heat of the above-mentioned liquid ^{3}He-^{4}He mixture. Moreover, we discuss possible similarities of the specific heat in the vicinity of the superfluid transition of *liquid ^{3}He* in the confinement of an Ag sinter with the results observed by other authors for the specific heat close to the superfluid transition of *liquid ^{4}He* confined to porous Vycor glass. In Sec. IV, the results are summarized. In the Appendix, the specific-heat data obtained for pure ^{3}He in the sinter of pore size $\sim$1000 Å at the two highest pressures ($p=25.2$ and 34.0 bar) are compared with the results obtained with ^{3}He restricted to a solid hcp ^{4}He matrix with a ^{3}He cluster size of $\sim$200 Å at comparable pressures ($p=26.5$ and 34.0 bar). A detailed report on the measurements in the latter geometry, which can only be achieved by applying a pressure $p>26$ bar in order to solidify ^{4}He, can be found in Refs. 7 and 8.

II. EXPERIMENTAL SETUP

The cylindrical cell body of the calorimeter was made of Ag (purity 99.999%) and annealed at 820 °C for 14 h. The Ag cell was then completely filled with an Ag sinter[9] compressed at about 400 bar resulting in a packing fraction $f\sim48\%$. This Ag sinter provides a surface area of 52 m^2 determined by Brunauer-Emmett-Teller adsorption isotherms with nitrogen gas at $T=77$ K.[10] As the cell is entirely filled with Ag sinter, the sample volume of 3.72 cm^3 is restricted to the pores and interconnecting channels of the sinter, i.e., there is no free (bulk) liquid volume in the cell around the sinter. The pore size of the sinter is estimated according to the sinter model suggested by Robertson, Guillon, and Harrison[11] (see also Ref. 12). Here, the open volume of a sinter is assumed as being made of cylindrical pores of the same diameter extending in three orthogonal dimensions and with intersections over part of their lengths. The diameter d of these cylindrical pores is then given by $d=4(1-f)/s$ with s being the surface area per unit volume. Using the above-given values for our experimental cell, we estimate a maximum pore size of the Ag of approximately 1500 Å.

The bottom of the calorimeter was formed by a Straty-Adams type capacitance strain gauge[13] to measure the pressure of the helium sample *in situ*. Titanium was chosen for the membranes because of its much smaller heat capacity compared with the commonly used BeCu. Calibration of the pressure gauge was performed at 4 K with an absolute accuracy of 10 mbar. The temperature of the calorimeter was measured by a Pt-NMR thermometer mounted on top of the cell and calibrated against the Curie susceptibility of a PdFe thermometer. The temperature scale is given by a National Bureau of Standards superconducting fixed-point device[14] with five superconducting transitions in the temperature range between $\sim$15 and $\sim$210 mK.

The calorimeter cell was supported and thermally isolated by three Vespel rods on the top flange of a $PrNi_5$ nuclear demagnetization stage. Thermal contact between the nuclear stage and the sample cell could be provided by a superconducting Al heat switch (three foils, $0.1\times10\times7$ mm^3). The Al foils were annealed and diffusion welded to an Ag support at 400 °C for 1 h. The switching ratio of the heat switch was $\kappa_n/\kappa_s=1.74\,\mathrm{T}^{-2}$, thus enabling good thermal isolation of the sample cell below 30 mK.

The specific heat was determined by the conventional heat pulse method. Heat was either supplied by an Ohmic heater glued to the wall of the calorimeter or, alternatively, by the heat input of the NMR pulses of the Pt-NMR thermometer; the energy input of the NMR pulses was calibrated against the Ohmic heater. We have performed various cross checks to prove the consistency between both ways of supplying heat to the calorimeter; in particular, we have varied length and excitation of the NMR pulses as well as the delay time between two pulses. The data are corrected for the heat capacity of the empty cell, which is about two orders of magnitude smaller than the heat capacity of the He samples at all temperatures of our experiment.

III. SPECIFIC HEAT OF NORMAL-FLUID AND SUPERFLUID ^{3}He AND OF A ^{3}He-^{4}He MIXTURE CONFINED TO THE PORES OF AN Ag SINTER

Figure 1 shows the specific heat of liquid ^{3}He at $p=4.8$, 15.5, 25.2, and 34.0 bar compared to data of bulk liquid ^{3}He (solid line) taken from Ref. 15. There are two distinct differences in the specific-heat data between liquid ^{3}He in the restricted geometry and the bulk liquid. (1) At all four pressures investigated in our experiment, the specific heat of normal-fluid ^{3}He is linearly dependent on temperature as it is in bulk ^{3}He, but the magnitude of the specific heat is enhanced compared with the bulk liquid data. (2) In bulk liquid ^{3}He, there is a distinct jump in the specific heat at the superfluid transition temperature T_C (by a factor of about 2.5) whereas we observe a rounding in the specific heat in the vicinity of the superfluid transition when the liquid is confined to the pores of the sinter, with an onset at $T_S^i<T_C$ and a maximum in the specific heat at $T_S^{\max}$ (throughout the context, the subscript S denotes the corresponding property of ^{3}He in the sinter).

A. Normal-fluid ^{3}He

In the normal-fluid regime the specific heat of liquid ^{3}He in the Ag sinter depends linearly on temperature but in contrast to the specific heat of bulk liquid ^{3}He there is a temperature-independent contribution to the specific heat, too (Fig. 2). A fit of

$$C=\gamma_S T+C_S \tag{1}$$

to our data provides the coefficient γ_S and the temperature-independent contribution C_S to the specific heat of ^{3}He in the pores of the sinter; for all pressures investigated these data are summarized in Table I. For comparison, the linear coefficient γ of the specific heat of bulk liquid ^{3}He obtained by Greywall[15] is listed, too. This value of γ is smaller than γ_S for all pressures investigated in our experiment.

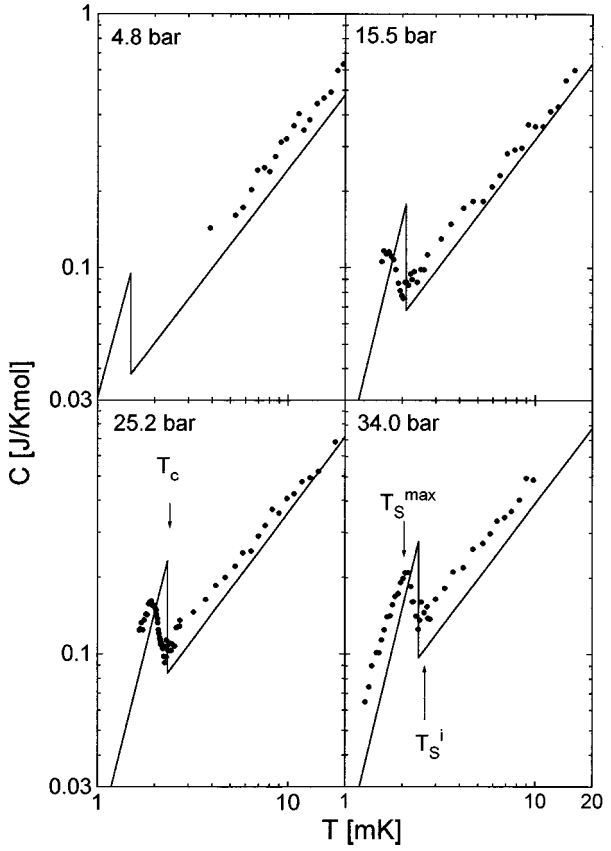

FIG. 1. Temperature dependence of the specific heat of liquid ^{3}He in an Ag sinter (●, this work) and of bulk liquid ^{3}He (solid line, from Ref. 15) at $p=4.8$, 15.5, 25.2, and 34.0 bar. T_C marks the superfluid transition temperature of bulk liquid ^{3}He, T_S^i the onset of the superfluid transition of liquid ^{3}He in the Ag sinter, and T_S^{max} the maximum of the specific heat of liquid ^{3}He in the Ag sinter.

The linear coefficient of the specific heat of a degenerate Fermi liquid provides information on the effective mass of the ^{3}He quasiparticles. According to Landau's Fermi-liquid theory, the specific heat of liquid ^{3}He is given by

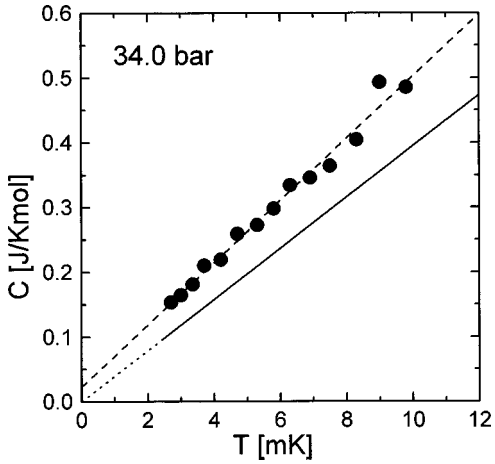

FIG. 2. Temperature dependence of the specific heat of normal-fluid liquid ^{3}He in an Ag sinter (●, this work) at 34.0 bar. The dashed line is a fit using Eq. (1) and the solid line represents the specific-heat data of bulk normal-fluid ^{3}He from Ref. 15. The dotted line is the extrapolation of the bulk data to $T=0$.

TABLE I. The coefficient γ_S and the temperature independent contribution C_S of the specific heat of liquid ^{3}He confined to an Ag sinter obtained from Eq. (1): m_S^*/m_3 is the ratio of the effective mass of the ^{3}He quasiparticles in the Ag sinter to the bare mass of a ^{3}He atom determined from the slope γ_S of the specific heat using Eq. (2). For comparison, the coefficient γ and the ratio m^*/m_3 of bulk liquid ^{3}He (Ref. 15) are listed.

p (bar)	4.8	15.5	25.2	34.0
γ (J/K^2 mole)	25.6	30.3	34.2	37.7
γ_S (J/K^2 mole)	30.8	34.6	37.4	48.0
m^*/m_3	3.36	4.33	5.12	5.82
m_S^*/m_3	4.04	4.94	5.60	7.41
C_S (J/K mole)	0.011	0.015	0.020	0.023

$$C_{\mathrm{Fermi}}=\gamma_s T=\frac{\pi^2 N_A k_B^2 m_3}{h/2\pi}\,\frac{m_3^*}{m_3}\,(V_m/3\pi^2 N_A)^{2/3}T. \quad (2)$$

Here, V_m is the molar volume of liquid ^{3}He, N_A is Avogadro's constant, k_B is Boltzmann's constant, h is Planck's constant, m_3 is the mass of a bare ^{3}He atom, and m_3^* is the effective mass of the ^{3}He quasiparticles. Figure 3 shows the effective masses of ^{3}He quasiparticles derived from our data of liquid ^{3}He confined to an Ag sinter (see also Table I). The effective mass of ^{3}He in the sinter is enhanced by up to about 20% compared with the effective mass of ^{3}He without restriction in geometry.[15] Moreover, we would like to point out that the effective mass at $p=34.0$ bar ($m_3^*/m_3=7.41$) is much larger than the value for the effective mass of bulk ^{3}He at the melting curve [$m_3^*/m_3=5.85$ (Ref. 15)], which is the largest effective mass observed in bulk liquid ^{3}He.

An enhancement of the effective mass of ^{3}He quasiparticles has been observed in various restricted geometries by other authors, too. For example, the effective mass of ^{3}He quasiparticles in clusters of size of $\sim$1000 Å embedded in a solid hcp ^{4}He matrix was found to be substantially larger

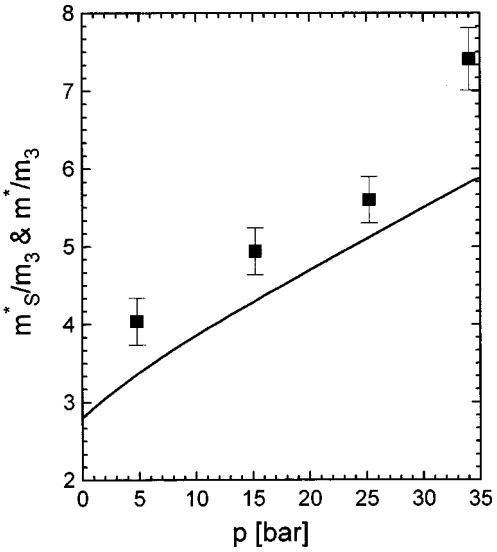

FIG. 3. Pressure dependence of the effective mass of liquid ^{3}He in the Ag sinter (■), compared with the effective mass of bulk liquid ^{3}He from Ref. 15.

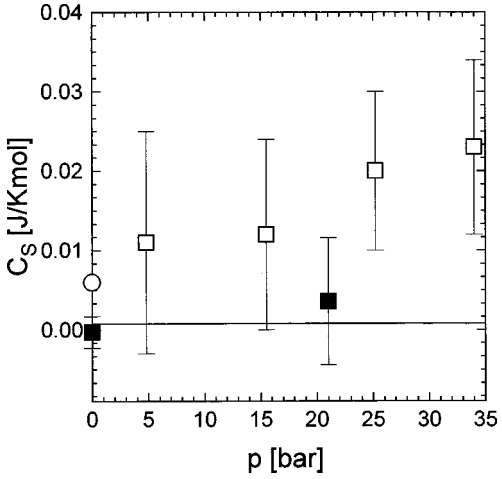

FIG. 4. The temperature independent contribution C_S to the specific heat of pure ^{3}He (□) and of a ^{3}He-^{4}He mixture with 1% ^{3}He (■) in the Ag sinter. For comparison, the heat capacity of the second layer of ^{3}He adsorbed on the surface of the Ag sinter at saturated vapor pressure (○), calculated from Ref. 16, is shown.

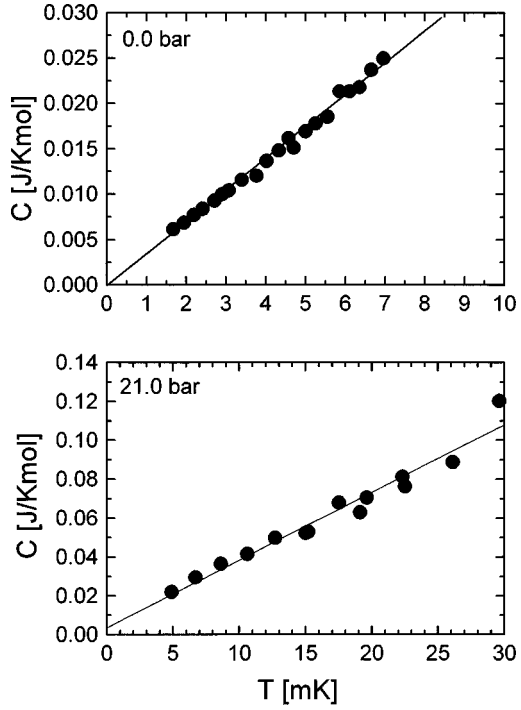

FIG. 5. Temperature dependence of the specific heat of a liquid ^{3}He-^{4}He mixture with a ^{3}He concentration of 1% in an Ag sinter at saturated vapor pressure and at $p=21.0$ bar; the solid line is a fit using Eq. (1). Note the different scales in temperature and specific heat.

than the effective mass of bulk ^{3}He.[4] Greywall and Busch interpreted their increased specific heat data on two-dimensional ^{3}He films on an Ag substrate as the result of a second-layer liquid with a very low Fermi temperature, which implies a ratio $m_3^*/m_3>300$.[16] Because the effective mass of ^{3}He quasiparticles is a measure of the interaction among them, one may conclude from these results, that a restriction in geometry leads to an increase in the density of states at the Fermi surface and thus in the interaction among the ^{3}He quasiparticles.

Concerning the temperature-independent contribution C_S to the specific heat of pure ^{3}He (Fig. 4 and Table I), one possible interpretation could be in terms of the specific heat of the second layer of ^{3}He on the Ag surface. According to Greywall and Busch,[16] the first layer of ^{3}He on the Ag surface is assumed to be solid, and its specific heat is negligibly small in the temperature range of our measurements. The specific heat of the second layer is reported to be temperature independent, and—normalized to the Ag surface of our experiment—its magnitude is comparable to the temperature-independent contribution C_S observed in our experiment (Fig. 4). Greywall and Busch suggested the second layer of ^{3}He to be a highly condensed Fermi liquid with a Fermi temperature smaller than 10 mK. Therefore, their measurements were not performed in the degenerate regime of this Fermi liquid, thus leading to a temperature-independent specific heat down to several mK. A different explanation for a temperature independent specific heat of the second layer of ^{3}He on the Ag surface is given by Golov and Pobell.[17] These authors consider the second layer as being solid with a continuous distribution of the exchange parameter J as a result of the roughness of the Ag surface leading to a temperature-independent specific heat.

B. ^{3}He-^{4}He mixture

Our measurements of the specific heat of a liquid ^{3}He-^{4}He mixture with a nominal ^{3}He concentration $x_3=1.0\%$ at two different pressures ($p=0$ and 25.2 bar, see Fig. 5) support the interpretations of the pure ^{3}He data described above. At both pressures, we again observe a specific heat characteristic for a Fermi liquid with its linear temperature dependence. As in the case of pure ^{3}He in the Ag sinter we fitted the specific heat of the mixture using Eq. (1) and calculated the effective mass using Eq. (2) in its modified form for ^{3}He-^{4}He mixtures.[5] However, in contrast to the behavior of pure ^{3}He described above and shown in Figs. 1 and 2, there is neither a difference in the effective masses of the ^{3}He quasiparticles between the ^{3}He-^{4}He mixture in the sinter pores and of a bulk mixture with the same concentration,[18] nor is there—within the experimental error—an offset in the mixture data extrapolated to $T=0$ K, see Fig. 4. The effective mass of the ^{3}He quasiparticle of the mixture in the confining geometry ($m_3^*/m_3=2.36$ at saturated vapor pressure; $m_3^*/m_3=2.88$ at 21.0 bar) derived from the slope of the specific heat data in Fig. 5 is in agreement with the values obtained for a bulk mixture with almost the same concentration (Ref. 18, $x_3=1.0\%$; Ref. 19, $x_3=1.3\%$), see Fig. 6. It is also important to note that a gradual increase in the ^{3}He concentration x_3 within the first few layers from the wall (with a layer of pure ^{4}He on the sinter substrate[20]) into the liquid (^{3}He-^{4}He mixture) may lead to a change in the effective concentration of the mixture in the pores by only $\sim 5\%$ at most (i.e., from $x_3=1.0$ to 1.05%) and may be therefore neglected in our analysis.

At saturated vapor pressure the interaction between ^{3}He quasiparticles and the superfluid ^{4}He background in a bulk mixture manifests itself in an effective mass ratio $m_3^*/m_3 \sim 2.3$ for the ^{3}He concentration x_3 extrapolated to zero.[18] This ratio increases only very slightly to about 2.36 for a

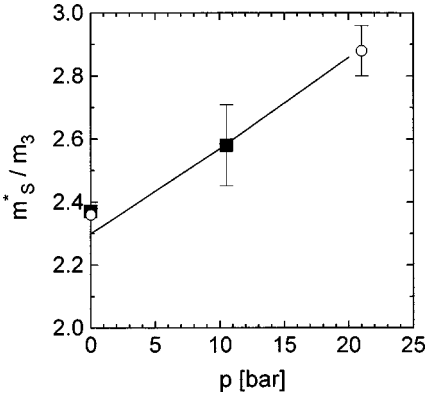

FIG. 6. The effective mass of a ^{3}He-^{4}He mixture with a ^{3}He concentration $x_3 = 1.0\%$ in an Ag sinter (○, this work) compared with data for bulk mixtures [solid line, Ref. 18; ■, Ref. 19 ($x_3 = 1.3\%$)].

^{3}He-^{4}He mixture with $x_3 = 1\%$ due to the interaction among the ^{3}He quasiparticles, i.e., the increase in the effective mass due to the *^{3}He-^{3}He quasiparticle interaction in the bulk liquid mixture* is only approximately 5% of the whole effective mass (^{3}He-^{3}He and ^{3}He-^{4}He). Therefore, it is obvious that an increase in the effective mass caused by an increase in the ^{3}He-^{3}He *quasiparticle interaction* of up to 20% due to the restricted geometry as it was observed for pure ^{3}He is beyond the resolution of our experiment.

Within experimental error, we do not observe a temperature-independent contribution to the specific heat in our measurements on the ^{3}He-^{4}He mixtures (see Fig. 4), which can be explained as follows: because of the smaller zero-point motion of the ^{4}He atoms the first two layers on the Ag surface are built up from ^{4}He atoms. The specific heat of solid ^{4}He layers is negligibly small compared to the specific heat of the ^{3}He-^{4}He mixture and so C_S should be zero for ^{3}He-^{4}He mixtures in sinter pores, if it is caused by the second layer on the sinter surface.

C. Superfluid ^{3}He

In contrast to bulk ^{3}He,[15] we do not observe a sharp peak but a broad maximum in the specific heat of ^{3}He confined to the Ag sinter (Fig. 7) at a temperature below the superfluid transition temperature of the bulk liquid. With decreasing temperature the specific heat of ^{3}He in the sinter starts to increase at a temperature T_S^i and shows a maximum at $T_S^{\max}$ (Table II), which is below the bulk transition temperature at all pressures investigated. The width of this rounding in the specific heat extends over several hundred μK, and it is therefore impossible to extract a single phase transition temperature T_C for ^{3}He in the Ag sinter. Finally, the magnitude of the specific heat at $T_S^{\max}$ is much smaller compared with the value obtained in bulk ^{3}He at T_C.

Similar features of an influence of a restricted geometry on the specific heat at the superfluid transition have been observed for liquid ^{4}He confined to porous Vycor glass, where in contrast to the sharp peak of the bulk liquid, a rounding of the specific heat (along with a reduced magnitude) of ^{4}He-filled pores at a temperature close to the bulk transition temperature is observed.[21] The particular importance of the liquid ^{4}He/Vycor system consists of the fact that it constitutes a model system for the study of the superfluid phase transition in a restricted geometry. In a number of experiments particular emphasis is given to the question of the dimensionality of the transition of liquid ^{4}He (films as well as full pores) in Vycor.[22] Concerning the specific heat of ^{4}He-filled Vycor, a maximum occurs very close to the bulk transition temperature,[21] in contrast, the onset of superfluidity of ^{4}He in Vycor is observed at significantly lower temperatures.[23] The observation of an anomaly in the specific heat of the ^{4}He/Vycor system at the superfluid transition failed until now despite considerable improvements in high-precision calorimetry.[24] A direct comparison between the results obtained for the specific heat of the liquid ^{4}He/Vycor experiments and the liquid ^{3}He/Ag sinter data, however, seems to be difficult because of the following important differences between both systems: the uniformity and the pore size distribution as well as the pore sizes themselves ($\sim$70 Å in Vycor and $\sim$1000 Å in the Ag sinter). Although

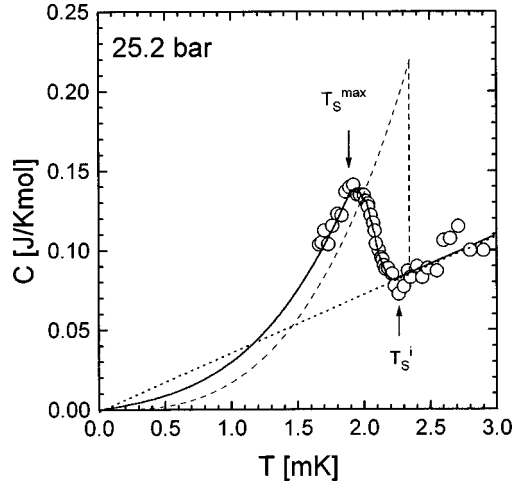

FIG. 7. Temperature dependence of the specific heat of liquid ^{3}He in an Ag sinter at 25.2 bar; T_S^i marks the onset of the superfluid phase transition; $T_S^{\max}$ is the temperature at which the specific heat has its maximum value. The solid line is the calculated specific heat as described in the text. For comparison, the specific heat of bulk ^{3}He (dashed line) and of normal-fluid ^{3}He in the Ag sinter extrapolated to $T = 0$ (dotted line) is plotted. The temperature-independent contribution to the specific heat that is related to the second layer of ^{3}He on the sinter surface is already subtracted from the data.

TABLE II. The superfluid phase transition temperature T_C of bulk ^{3}He (Ref. 15) compared with T_S^i (onset of the increase of the specific heat) and $T_S^{\max}$ (maximum of the specific heat) of liquid ^{3}He confined to an Ag sinter. The superfluid fraction n of liquid ^{3}He in the sinter is calculated from the specific-heat data; $\xi(T_S^{\max})$, $\xi(T_S^i)$ are the coherence lengths at $T_S^{\max}$ (T_S^i).

p (bar)	15.5	25.2	34.0
T_C (mK)	2.05	2.36	2.47
T_S^i (mK)	1.94	2.23	2.37
$T_S^{\max}$ (mK)	1.60	1.95	2.10
n (%)	64±5	63	53
$\xi(T_S^{\max})$ (Å)	470±30	480	440
$\xi(T_S^i)$ (Å)	950±100	852	845

we do not have any detailed information about the pore size distribution in the sinter, we may explain the presence of a large pore size distribution as resulting from the particle size distribution of the Ag powder: a Gaussian fit to the particle size distribution as provided by the manufacturer[9] results in a maximum at ~ 850 Å with a width of ~ 650 Å; these data might be considered as lower limits as the Ag powder is known to form larger clusters due to sintering processes even at room temperature.[25]

For an interpretation of the specific heat results in the vicinity of the superfluid transition obtained for our ^{3}He samples in the confinement of the Ag sinter, we discuss our data in more detail as it is illustrated in Fig. 7 by means of the measurements at $p = 25.2$ bar. In this figure, the temperature-independent contribution C_S has already been subtracted from the data leading to zero heat capacity for the extrapolated normal-fluid data (dotted line) at $T = 0$ K. We assume that in each pore of the sinter the transition temperature is determined by the size of the pore; the smaller the pore, the lower the T_C. The distribution of the pore sizes in the sinter then leads to different phase transition temperatures in the temperature range $T_S^{\max} \leqslant T \leqslant T_S^i$. We have fitted the data by varying the amount of ^{3}He, which becomes superfluid at a certain temperature T using the specific heat data of normal-fluid ^{3}He in the sinter with the enhanced effective mass as listed in Table I. Further important underlying assumptions of our analysis (thus neglecting a possible correspondence to the findings of the specific heat in the liquid ^{4}He/Vycor system as discussed above) are that the specific heat of the superfluid ^{3}He in the sinter shows the same temperature dependence as bulk ^{3}He (Ref. 15) and that in all pores of same size the jump in the specific heat at the superfluid transition is of equal size as the jump observed in the bulk liquid.

This analysis of the specific heat provides an interesting result, which might explain some experimental observations obtained in investigations of other ^{3}He properties: the best fit (solid curve) to the data in Fig. 7 is obtained with only a fraction of the ^{3}He in the Ag sinter becoming superfluid (Table II), the remainder staying normal-fluid down to the lowest temperature achieved in our experiment. According to this analysis, about 40% of the ^{3}He in the sinter remains normal-fluid and this amount should have an important influence on various properties as, e.g., the thermal conductivity of the liquid in the sinter or the thermal boundary resistance between liquid ^{3}He and the sinter. Measurements of the thermal boundary resistance, for instance, performed by Ahonen, Lounasmaa, and Veuro[26] in the temperature range $0.4 \leqslant T \leqslant 10$ mK do not show a change in the temperature dependence even at the superfluid transition. This result could be interpreted in terms of a normal-fluid component near the wall of the sinter, which dominates the thermal boundary resistance.

Within experimental error, the superfluid fraction of ^{3}He in the Ag sinter seems to be pressure independent (see Table II), in contrast to the observation of a decreasing superfluid density with decreasing pressure obtained by torsional oscillator measurements of Hall *et al.*[12] These authors related the decrease in superfluid density with decreasing pressure to the increase of the coherence length at lower pressure. However, another explanation for a pressure-independent superfluid fraction is given by the following arguments.

The coherence length at a distinct temperature can be calculated according to

$$\xi(T,p) = \xi_0(p) \cdot \left(1 - \frac{T}{T_C(p)}\right)^{-1/2}, \tag{3}$$

where ξ_0 is the zero-temperature coherence length given by

$$\xi_0(p) = \frac{h v_F(p)}{2\pi k_B T_C(p)}. \tag{4}$$

The pressure dependences of the Fermi velocity v_F and of the transition temperature T_C result in a pressure dependence of the zero-temperature coherence length ξ_0, too. The coherence lengths at the characteristic temperatures T_S^i and $T_S^{\max}$ calculated with Eq. (3) and Eq. (4), however, do not exhibit a pressure dependence within the experimental error of our measurement; see Table II. From our data one may therefore conclude that independent on the pressure of the sample the onset of the increase of the specific heat (at T_S^i) and the onset of the superfluid phase transition of ^{3}He in the sinter occurs at a temperature where the coherence length of superfluid ^{3}He is about 900 Å, which is close to the radius of our sinter pores. It is interesting to note that the difference ΔT between the bulk transition temperature T_C and the temperature T_S^i at which the specific heat starts to increase is almost constant [$\Delta T = (0.11 \pm 0.01)$ mK]. The striking agreement of this result with the findings of a torsional oscillator experiment of Tholen[27] in which a shift of the superfluid transition of liquid ^{3}He in an Ag sinter of $\Delta T = 0.10$ mK ($p = 5$ bar), 0.17 mK ($p = 17$ bar), 0.10 mK ($p = 24$ bar) and 0.11 mK ($p = 28$ bar) compared to the bulk value was observed, could be interpreted as an indication for a different behavior at the superfluid transition of ^{3}He in the sinter compared with the transition of ^{4}He in Vycor (see discussion at the beginning of Sec. III C). The maximum of the specific heat (at $T_s^{\max}$) is related to a pressure-independent coherence length of about 470 Å. We may therefore conclude that the amount of ^{3}He that undergoes the superfluid phase transition does not depend on the pressure of the sample.

Kjäldman, Kurkijärvi, and Rainer[28] have calculated the suppression of the transition temperature of superfluid ^{3}He as a function of the size of an infinitely long cylindrical pore with diffusely scattering walls. Figure 8 shows the fractional depression of T_s^i and $T_s^{\max}$ in the Ag sinter as a function of pressure, compared to the theoretical curves obtained from the work of Kjäldman, Kurkijärvi, and Rainer using cylindrical pores of radius 600 and 1200 Å, respectively. Although the sinter structure is much more complicated than an ideal cylindrical form, we find good agreement in the pressure dependence between the theoretical and experimental results with values for the pore size which are comparable to our estimate of the pore size according to Ref. 8.

IV. SUMMARY

We have studied the specific heat of liquid ^{3}He confined to an Ag sinter at pressures $4.8 \leqslant p \leqslant 34.0$ bar and in the temperature range $1 \leqslant T \leqslant 30$ mK. The measured specific

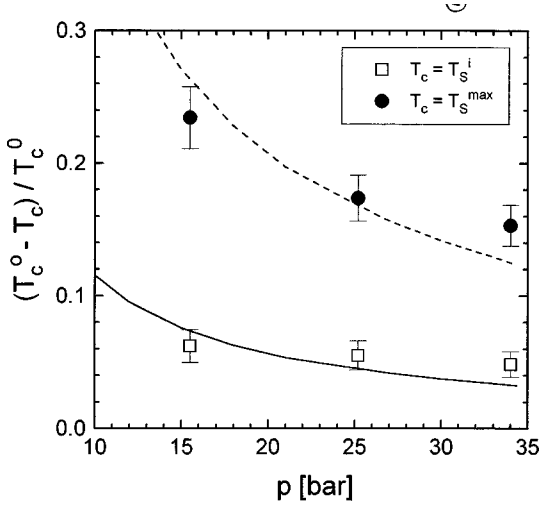

FIG. 8. Fractional depression of the superfluid transition temperatures assuming $T_C = T_S^i$ (□) and $T_C = T_S^{max}$ (●) in the Ag sinter as a function of pressure. T_C^0 is the superfluid phase transition temperature of bulk ^{3}He. The lines are theoretical curves for the fractional depression of the superfluid transition temperature in cylindrical pores with radii of 600 Å (dashed line) and 1200 Å (solid line) (Ref. 21).

heat of normal-fluid ^{3}He in the confinement of the sinter pores shows enhanced values compared to bulk data. This increase can be explained as being the result of two contributions: (1) an enhanced effective mass of the quasiparticles in the restricted geometry of up to 20% of its value in the bulk liquid and (2) an additional temperature-independent part originating from the second layer of ^{3}He on the substrate. Due to the much weaker interaction among the ^{3}He quasiparticles in a liquid ^{3}He-^{4}He solution, we do not observe these features in our measurements of the specific heat of a mixture with the nominal ^{3}He concentration $x_3 = 1.0\%$. The transition into the superfluid phase of ^{3}He is strongly influenced by the confinement, too. In contrast to the bulk data, there is a much broader maximum in the specific heat for the liquid in the restricted geometry, and the position of the maximum is shifted to lower temperatures compared with the bulk transition temperature. We analyze our specific-heat data in the vicinity of the maximum in terms of phase transitions in the sinter pores with different transition temperatures determined by the coherence length and the sinter pore size. We conclude that only a fraction of ~60% of ^{3}He becomes superfluid in the Ag sinter.

APPENDIX: INFLUENCE OF THE CLUSTER SIZE ON THE SPECIFIC HEAT

As discussed in the previous sections, when confined to the restricted geometry of an Ag sinter with an average pore size of about 1000 Å, the specific heat of normal-fluid ^{3}He can be described by Landau's theory for a Fermi liquid with an enhanced effective mass and a temperature-independent contribution arising from the second layer of ^{3}He on the substrate. The broadening of the transition into the superfluid phase can be related to the pore size, too. The observed features clearly indicate that the restriction to the dimension of

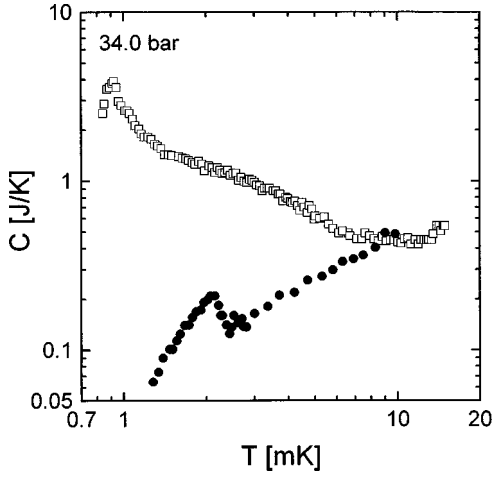

FIG. 9. Temperature dependence of the specific heat of ^{3}He clusters in solid hcp ^{4}He (□) (Refs. 7 and 8) and of ^{3}He in an Ag sinter (●, this work) at $p = 34.0$ bar.

~1000 Å does not alter the phase (liquid or solid) significantly.

The situation becomes completely different when the confinement is further reduced to smaller geometries and the confining material is different from a metal sinter. We have performed measurements of the specific heat of clusters of ^{3}He confined to pores in a matrix of solid hcp ^{4}He which in turn is restricted to an Ag sinter. The size of these ^{3}He clusters is estimated to be of order of 200 Å. In this appendix, we present a brief comparison of the very different behavior of ^{3}He confined to both geometries. For detailed results on the measurements of the specific heat in the latter geometry, the reader is referred to Refs. 7 and 8. At $p = 34.0$ bar the specific heat of the ^{3}He clusters differs completely from the specific heat of liquid ^{3}He in the Ag sinter (Fig. 9). At $T < 10$ mK, we observe an increasing specific heat of the ^{3}He clusters with decreasing temperature with a maximum at around 1 mK, where the specific heat is about two orders of magnitude larger than the specific heat of ^{3}He in the Ag sinter. The specific heat of the ^{3}He clusters is dominated by solid ^{3}He even at pressures significantly below

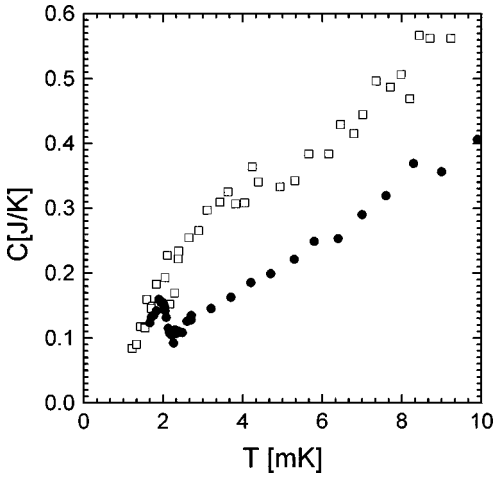

FIG. 10. Temperature dependence of the specific heat of ^{3}He clusters in solid hcp ^{4}He at $p = 26.5$ bar (□) (Refs. 7 and 8) and of ^{3}He in an Ag sinter (●, this work) at 25.2 bar.

the bulk ^{3}He melting pressure ($p_{\mathrm{melt}}=34.4$ bar at $T=1$ mK) and the maximum indicates the nuclear magnetic ordering of the solid ^{3}He in the clusters.

The situation changes at lower pressure of the sample (26 bar; Fig. 10). Both the specific heat of the ^{3}He clusters and the specific heat of ^{3}He in the Ag sinter now show the linear temperature dependence of a Fermi liquid. However, in contrast to ^{3}He in the Ag sinter there is no sign for a superfluid phase transition of the ^{3}He in the clusters and the specific heat of the normal-fluid ^{3}He in the clusters is larger than the specific heat of ^{3}He in the sinter resulting in a larger effective mass (^{3}He cluster, $m^*_{\mathrm{cluster}}/m_3=8.4$ at $p=26.5$ bar; ^{3}He in the Ag sinter, $m^*_{\mathrm{sinter}}/m_3=5.6$ at $p=25.2$ bar).

ACKNOWLEDGMENTS

We are very grateful for the support of and discussions with Professor F. Pobell. This work was supported by the HCM Large Scale Facility program of the European Community (Contract No. ERBCHGE-CT 92-0002) and by the Graduiertenkolleg Po88/13 of the Deutsche Forschungsgemeinschaft.

*Present address: Hahn-Meitner Institut Berlin, Glienicker Straße 100,
D-14109 Berlin, Germany.

[1] L. D. Landau, Sov. Phys. JETP **3**, 920 (1957).
[2] See for example, *The Physics of Liquid and Solid Helium*, edited by K. H. Benneman and J. B. Ketterson (Wiley, New York, 1976 and 1978), Vols. I and II.
[3] T. Chainer, Y. Morii, and H. Kojima, Phys. Rev. B **21**, 3941 (1980); V. Kotsubo, K. D. Hahn, and J. P. Parpia, Phys. Rev. Lett. **58**, 804 (1987); J. Xu and B. C. Crooker, *ibid.* **65**, 3005 (1990).
[4] B. Hébral, A. S. Greenberg, M. T. Béal-Monod, M. Papoular, G. Frossati, H. Godfrin, and D. Thoulouze, Phys. Rev. Lett. **46**, 42 (1980); E. Syskakis, Y. Fujii, F. Pobell, and H. Schroeder, J. Low Temp. Phys. **79**, 341 (1990).
[5] For a review of the properties of liquid ^{3}He-^{4}He mixtures, see, for example, C. Ebner and D. O. Edwards, Phys. Rep., Phys. Lett. **2C**, 77 (1971).
[6] G. E. Watson, J. D. Reppy, and R. C. Richardson, Phys. Rev. **188**, 384 (1969).
[7] R. Schrenk, R. König, and F. Pobell, Phys. Rev. Lett. **76**, 2945 (1996).
[8] R. Schrenk and R. König (unpublished).
[9] Ag powder: Inabata Corp., Vacuum Metallurgical Ltd., Japan (nominal grain size 700 Å).
[10] S. Brunauer, P. H. Emmett, and E. Teller, J. Am. Chem. Soc. **60**, 309 (1938).
[11] R. J. Robertson, F. Guillon, and J. P. Harrison, Can. J. Phys. **61**, 164 (1983).
[12] T. Hall, S. M. Thoulen, K. R. Lane, V. Kotsubo, and J. M. Parpia, J. Low Temp. Phys. **89**, 897 (1992).
[13] G. S. Straty and E. D. Adams, Rev. Sci. Instrum. **40**, 1393 (1969).
[14] F. Pobell, *Matter and Methods at Low Temperatures* (Springer-Verlag, Berlin, 1992), p. 204, and references therein.
[15] D. S. Greywall, Phys. Rev. B **33**, 7520 (1986).
[16] D. S. Greywall and P. Busch, Phys. Rev. Lett. **60**, 1860 (1988).
[17] A. Golov and F. Pobell, Phys. Rev. B **53**, 12 647 (1996).
[18] S. Yorozu, M. Hiroi, H. Fukuyama, H. Akimoto, H. Ishimoto, and S. Ogawa, Phys. Rev. B **45**, 12 942 (1992).
[19] H. C. Chocholacs, R. M. Mueller, J. R. Owers-Bradley, Ch. Buchal, M. Kubota, and F. Pobell, in *Proceedings of the 17th International Conference of Low Temperature Physics*, edited by U. Eckern, A. Schmid, W. Weber, and H. Wuhl (North-Holland, Amsterdam, 1984), p. 1247.
[20] See, e.g., J. P. Harrison, J. Low Temp. Phys. **37**, 467 (1979); S. M. Tholen and J. M. Parpia, Phys. Rev. Lett. **68**, 2810 (1992).
[21] D. F. Brewer, J. Low Temp. Phys. **3**, 205 (1970).
[22] See, e.g., J. D. Reppy, J. Low Temp. Phys. **87**, 205 (1992), and references therein.
[23] See, e.g., C. W. Kiewiet, H. E. Hall, and J. D. Reppy, Phys. Rev. Lett. **35**, 1286 (1975); M. H. W. Chan, K. I. Blum, S. Q. Murphy, G. K. S. Wong, and J. D. Reppy, *ibid.* **61**, 1950 (1988); A. Tyler, H. A. Cho, and J. D. Reppy, J. Low Temp. Phys. **89**, 57 (1992).
[24] G. M. Zassenhaus, A. Tyler, and J. D. Reppy, Czech. J. Phys. Suppl. S1 **46**, 147 (1996).
[25] H. Franco, J. Bossy, and H. Godfrin, Cryogenics **24**, 477 (1984).
[26] A. I. Ahonen, O. V. Lounasmaa, and M. C. Veuro, J. Phys. (Paris), Colloq. **C6**, 265 (1978).
[27] S. M. Tholen, Ph.D. thesis, Cornell University, 1992; see also Ref. 12 and second reference in Ref. 20.
[28] L. H. Kjäldman, J. Kurkijärvi, and D. Rainer, J. Low Temp. Phys. **33**, 577 (1978).